

RSC Advances



This is an *Accepted Manuscript*, which has been through the Royal Society of Chemistry peer review process and has been accepted for publication.

Accepted Manuscripts are published online shortly after acceptance, before technical editing, formatting and proof reading. Using this free service, authors can make their results available to the community, in citable form, before we publish the edited article. This *Accepted Manuscript* will be replaced by the edited, formatted and paginated article as soon as this is available.

You can find more information about *Accepted Manuscripts* in the [Information for Authors](#).

Please note that technical editing may introduce minor changes to the text and/or graphics, which may alter content. The journal's standard [Terms & Conditions](#) and the [Ethical guidelines](#) still apply. In no event shall the Royal Society of Chemistry be held responsible for any errors or omissions in this *Accepted Manuscript* or any consequences arising from the use of any information it contains.

Ammonolytical conversion of microcrystalline gallium antimonide GaSb to nanocrystalline gallium nitride GaN: thermodynamics vs. topochemistry.

Mariusz Drygaś^{1a}, Piotr Jelen^{1b}, Mirosław M. Bućko^{1b}, Zbigniew Olejniczak², Jerzy F. Janik^{1a*}

¹AGH University of Science and Technology, ^aFaculty of Energy and Fuels, ^bFaculty of Materials Science and Ceramics; al. Mickiewicza 30, 30-059 Krakow, Poland.

²Institute of Nuclear Physics, Polish Academy of Sciences; Radzikowskiego 152, 31-342 Krakow, Poland.

*Corresponding author. E-mail: janikj@agh.edu.pl

Abstract. Reactions of microcrystalline powders of the readily available gallium antimonide GaSb with ammonia gas at elevated temperatures afforded in one step high yields of nanocrystalline powders of the gallium nitride GaN semiconductor. In particular, temperatures at 900-1000 °C and suitable 36 to 170-hour reaction times resulted in complete nitridation in the system. The nitride was made as a mixture of the major stable hexagonal and the minor metastable cubic polytypes. Formation of the cubic GaN was consistent with topochemistry playing a meaningful role in ammonolysis of the cubic GaSb substrate. Specific experimental conditions including variations of the reaction temperature/time and manual grinding or high energy ball milling of the substrate had an essential impact on final GaN polytype make-up and average crystallite sizes, the latter ranging from a few to a few tens of nanometers. Under the applied conditions, all by-products were conveniently removed from the reaction zone as volatile species affording chemically pure GaN nanopowders of very good quality.

Keywords: gallium antimonide, gallium nitride, ammonolysis, nanopowders

1. Introduction

Gallium nitride GaN has become an indispensable part of modern electronics thanks to its attractive and unique features including advantageous semiconducting properties. The wide bandgap of 3.4 eV makes hexagonal GaN suitable for diverse optoelectronic applications to mention the detection and emission of light in the blue and ultraviolet ranges. The nitride's feasibility to form solid solutions with other Group III(13)-nitrides, additionally, being doped with suitable carriers/centers creates conditions for effective modifications of the material's all-in-one semiconducting, optical, and magnetic properties.

There are numerous methods reported for the synthesis of GaN most of which are concerned with the seminal thin films applications in light-emitting devices.¹ Recently, for similar reasons monocrystalline gallium nitride technologies have also received due attention.² It appears, however, that the knowledge about reproducible synthesis methods and unequivocal properties of nanocrystalline powders of Group III(13) nitrides including the GaN semiconductor is not yet satisfactory as exemplified by some reviews.³ In general terms, the synthesis methods are based here mostly on reactions of the affordable gallium metal or gallium oxygen-bearing compounds with a nitriding agent (*e.g.*, ammonia, nitrogen) whereas, sometimes, more elaborate organometallic gallium precursors are also tried.

Some of the authors of this report contributed to developing a few synthesis routes to GaN nanopowders such as the metathesis of gallium halides and lithium nitride,⁴ nitriding decomposition of gallium imide⁵ and cyclotrigalazane⁶ as well as aerosol-assisted ammonolysis of gallium nitrate solutions.^{5g-i,7} Regarding our studies, one can stress advantages of the anaerobic gallium imide route that yields in an easily controlled way average crystallite sizes of GaN ranging from one to several tens of nanometers and of the aerosol-assisted method that uses the affordable gallium nitrate precursor in a relatively large-scale synthesis of particles with spherical morphology. However, the gallium imide route is a

tedious multi-stage process requiring all the elaborate equipment/techniques and precautions characteristic of anaerobic syntheses. In turn, the aerosol-assisted route is a two-step synthesis resulting, typically, in crystallite sizes above 30 nm and suffering from chances of getting residual oxygen in the product. Actually, there are various shortcomings in all known to us methods to warrant economical supplying of large quantities of pure and size-controlled nanopowders of GaN. In this regard, a synthesis scale-up aspect has become troublesome for us in the otherwise successful attempts to optimize our high-temperature high-pressure sintering of GaN nanopowders into robust and machinable ceramics.⁸ Hence, we learned first-hand that there is still a need for an economical and well-controlled method of GaN nanopowder synthesis.

In our initial attempt to accomplish such a goal, we have re-examined reactions of gallium arsenide GaAs with ammonia which appeared to be especially well suited for synthesis of the rare GaN cubic polytype, c-GaN.⁹ The latter variety was shown to be made there in up to 90 % yield in admixture with the GaN hexagonal polytype, h-GaN. It is worth mentioning that, thermodynamically, c-GaN is a metastable phase so that its predominant formation could be linked to favorable topochemical conditions set-up during ammonolysis with N for As replacements in the cubic lattice of the substrate GaAs. For instance, topochemical circumstances were invoked in explaining GaN polytype make-up in the pyrolysis of cyclotrigallazane.¹⁰ In summary of our research, the GaAs/NH₃ system was proved to efficiently yield gallium nitride nanopowders, however, with enhanced proportions of the cubic polytype. In extending this idea, the related gallium pnictides such as gallium antimonide GaSb and gallium phosphide GaP have been subjected to similar chemistry in our laboratory confirming the general trend and the results will be published elsewhere.

This report describes the synthesis of nanocrystalline GaN by ammonolysis of microcrystalline gallium antimonide GaSb. Specifically, monocrystalline chunks of GaSb

were either manually ground in an agate mortar or milled in a high energy ball mill, which was followed by pyrolysis under a flow of ammonia for up to 170 hours at temperatures in the 800-1000 °C range. The products encompassed yellowish (lower temperatures) to gray yellowish (higher temperatures, longer times) powders that were thoroughly characterized.

2. Experimental

Synthesis. Post processing chunks of GaSb of commercial quality were acquired as waste material from the Institute of Electronic Materials Technology, Warszawa, Poland. The material required grinding that was accomplished with two different methods. In manual grinding, several grams of chunks were placed in an agate mortar and ground for approximately 10 minutes to afford a gray powder. For deep grinding by a standard wet high energy ball milling, a few grams of chunks crashed to sizes below *ca.* 1 mm were placed in a grinding bowl of the FRITSCH Pulverisette 7 planetary ball mill onto which 10 ml of dry xylene were added. Twenty 3-minute intermittent grinding periods were applied at 900 rpm, each separated with a 10-minute break to prevent overheating of bowl's content. After each grinding period, the bowl warmed-up to 50-60 °C much below the boiling point of xylene, 140 °C. Following recovery from the bowl, the sticky paste was evacuated for 1 h to remove volatiles affording an agglomerated gray precursor powder. A batch of 1 to 2 grams of powder was placed in an alumina boat and inserted into a continuous ceramic reactor in a tube furnace. Prior to heating, the system was purged with high purity ammonia, 99.999 %, 30 minutes, 0.05 L/min, and such a flow rate was maintained throughout the reaction. A selected reaction temperature was attained with a heating rate of 5 °C/min. Preliminary experiments were carried out at 800 and 850 °C to afford the major unconverted GaSb, some elemental Sb, and mere traces of GaN. For the reaction at 900 °C, two hold times were used, *i.e.*, 90 and 170 hours with only the latter conditions affording complete nitridation in the system utilizing

manually ground GaSb. For the reaction at 1000 °C, a 36-h heating accomplished the same goal. An additional single experiment at 1050 °C, 6 h, proved also to be efficient. The reactions were carried out for both the manually ground and ball milled GaSb powders. Upon cooling to room temperature under flowing NH₃, each sample was evacuated for 30 minutes to remove volatiles. The final products were gray yellowish, loosely agglomerated powders.

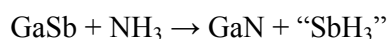
Characterization. Particle size distribution for substrate powders was measured by dynamic light scattering on Nanosizer-ZS of Malvern Instruments. All final products were characterized by standard powder XRD analysis (X'Pert Pro Panalytical, Cu K_α source; 2 Θ =10-110°). Average crystallite sizes were evaluated from Scherrer's equation applying the Rietveld refinement method. For the evaluation, changes of the line profile parameters compared to a standard sample were utilized. The profile parameters depend on the instrument settings used for data collection and on the profile function used for the refinement. In our analysis, the full Voigt function was used to describe the profile of the measured diffraction lines. The total profile width is a convolution of the Gaussian profile part and of the Lorentzian profile part and these parts are combined numerically. In such a method, the full width at half-maximum (fwhm) is only one of several fitted parameters. In a few cases of patterns containing severely overlapped peaks for different phases, the crystallite sizes were estimated from the strongest low angle peaks. X-ray fluorescence XRF determinations were performed on PANalytical WDXRF Axios mAX spectrometer equipped with a 4 KW Rh lamp. Solid-state ⁷¹Ga MAS NMR spectra of three series of samples were measured. The first two were acquired on the APOLLO console (Tecmag) at the magnetic field of 7.05 T produced by a 89 mm bore superconducting magnet (Magnex). A Bruker HP-WB high-speed MAS probe equipped with a 4 mm zirconia rotor and KEL-F cap was used to record the MAS NMR spectra at the spinning rates of 10 kHz. The resonance frequency was equal to 91.385 MHz and a single 2 μ s rf pulse was used, which corresponded to $\pi/4$ flip angle in the liquid.

The acquisition delay used in accumulation was 1 second and the typical number of acquisitions ranged from 1000 to 4000. The third series of samples was measured on the 500 MHz Bruker Avance III spectrometer, at 152.48 MHz. The spinning rate of the 3.2 mm MAS probe was equal to 20 kHz. A single 0.5 μ s rf pulse was used which corresponded to $\pi/4$ flip angle in the liquid. The acquisition delay used in accumulation was 5 seconds and 1000 scans were acquired. In all cases, the frequency scale in ppm was referenced to Ga(NO₃)₃ (1 M in D₂O). All resonance positions were uncorrected for the second-order quadrupolar shift. The comparison of spectra of one specific sample (900 °C, 170 h) measured at two frequencies shows that the second order quadrupolar effects are negligible. FT-IR spectra for KBr pellets were recorded with a Nicolet 380 spectrometer. Micro-Raman analysis was done by HORIBA LabRAM HR spectrometer with 532 nm laser, sample power of 20 mW, accumulation time 10 s and 2 scans, confocal hole 1000 μ m with long-focus length. UV-Vis data were collected on a Perkin-Elmer spectrophotometer Lambda 35 equipped with a 50 mm integrating sphere. SEM/EDX data were acquired with a Hitachi Model S-4700 scanning electron microscope.

3. Results and discussion

3.1. Chemistry, topochemistry, and thermodynamics in the system

The chemistry behind the metathetical nitridation of GaSb can be summarized by a simplified reaction mimicking a related case of the system GaAs/NH₃^{9c}



(ΔH_f^0 GaSb = -44 kJ/mol, ΔH_f^0 NH₃ = -46 kJ/mol, ΔH_f^0 GaN = -157 kJ/mol), where “SbH₃” denotes, in short, all volatile antimony species of unspecified nature. In this regard, stibine SbH₃ itself is a gas that is reported to be unstable at ambient conditions (ΔH_f^0 SbH₃ = 145 kJ/mol) decomposing to antimony Sb and hydrogen H₂.¹¹ For the actual reaction



the calculated standard reaction enthalpy is $\Delta H_r^0 = -67$ kJ/mol and, therefore, the ammonolysis of GaSb to GaN is thermodynamically supported.

The bulk elemental Sb has the melting point of 631 °C and the boiling point of 1635 °C. However, the nanosized Sb if formed would melt at significantly lower temperatures than that, possibly, showing sufficient volatility to be transported in the gas stream out of the reaction zone. In this regard, the partial vapor pressure of Sb at 712 °C, the melting point of GaSb, is *ca.* 10^{-6} atm which means that during extended reaction hours at high temperatures significant quantities of it could be lost/transported out.¹² Although, an exact mechanism of removing Sb from the system is unknown, the formation of elemental Sb and its persistence in the mixture with GaN, especially, at nitriding temperatures lower than 900 °C and relatively short reaction times is confirmed in this study (*vide infra*). At suitably high temperatures and long hold times neither GaSb nor Sb are any longer detected by XRD in the product powders. Also, all final nanopowders were examined by SEM/EDX and XRF to show no Sb within the methods detection limits.

It is worth noting that temperatures in the range 800-1000 °C employed here are higher than the melting point of GaSb. This may create a situation where surface nitridation with ammonia forms first GaN or transient GaSbN solid layers on otherwise liquid droplets of molten GaSb followed by a different, mostly, diffusion-controlled mechanism of droplets' molten interior nitridation. One may predict, therefore, that the substrate grain size should have a demonstrable effect on the reaction output. Anyhow, there was no evidence for bulk melting of the GaSb substrate and the products were loosely agglomerated GaN nanopowders.

Regarding the known chemistry of GaSb with nitrogen sources, available reports describe mostly the formation of GaSbN/GaN/Sb layers, often, on GaSb substrates *via* various gas or liquid phase-assisted deposition techniques. Such dilute nitride GaSbN/GaN/Sb structures are known to lead to a reduction of the band gap of GaSb opening the possibility of using the

material for long-wavelength applications. To this end, polycrystalline GaN with elemental Ga were used as nitrogen source and liquid phase, respectively, to form a GaSbN layer with 1 % nitrogen content on a GaSb monocrystal.^{13a} Hydrazine solutions were applied to the surface of a GaSb single-crystal wafer to make a postulated GaN monolayer on it.^{13b} Dilute nitride GaNSb layers with up to 1.4 % nitrogen of a few micrometer thickness were grown on GaSb substrates by MBE using a RF plasma nitrogen source.^{13c} Plasma-assisted MBE technique was used to grow dilute GaNSb films at temperatures 310-460 °C with up to 1.7 % nitrogen, the latter value being temperature dependent.^{13d} A recent review of these efforts, which includes electronic structure calculations in the dilute nitride alloy $\text{GaSb}_{1-x}\text{N}_x$, stresses a complex nature of nitrogen sites including a single N-incorporation on a Sb-site and a two nearest-neighbor N centers on the closest Sb sites.^{13e} One needs to underline that based on those reports for at least up to *ca.* 1.7 % of incorporated N the GaSbN/GaNSb lattice preserves the cubic symmetry of the substrate GaSb. Also, to the best of our knowledge, no reports on complete nitridation of GaSb and/or reactions of GaSb with NH_3 are available.

As far as the stability of the GaN polytypes is concerned, theoretical calculations suggest a very small difference in standard total energies between the hexagonal and cubic polytypes.¹⁴ The total energy of cubic GaN (c-GaN) is lower merely by 9.88 meV/atom or 16 meV/unit than for hexagonal GaN (h-GaN). These data imply that formation of the nitride's metastable cubic phase is fundamentally quite probable given the appropriate choice of reaction/experimental conditions (kinetic control, extreme pressure/temperature, substrate surface-nitride layer lattice compatibility, topochemistry, *etc.*). There are quite a few reports confirming the formation of pure c-GaN, mostly, as thin films or polycrystalline products from autoclave syntheses whereas under moderate conditions the synthesized c-GaN is often accompanied by the stable h-GaN either as a mixture of separate bulk phases or defect-related intra-growth of both lattice domains.

In this regard, a very interesting aspect of the system GaSb/NH₃ is a potential impact of the topochemical factor on GaN polytype formation. One could envision that under appropriate conditions antimony centers in the cubic GaSb would be gradually replaced with nitrogen (from ammonia decomposition) preserving the cubic lattice in the form of transient GaSbN and, eventually, producing a rare c-GaN. Such a transitional conversion of c-GaSb to c-GaN *via* a gradually collapsing cubic lattice is appealing since their *a* lattice constants, 6.1 and 4.5 Å, respectively, differ significantly to otherwise warrant the lattice type preservation. However, if thermodynamics prevails the stable h-GaN will be formed, instead.¹⁴ The latter scenario is likely to take place if molten GaSb reacts with ammonia or if it is preferentially decomposed to elements and the resulting liquid Ga (m.p. 30 °C) is then nitrided towards GaN. Therefore, in order to increase chances for c-GaN formation one should minimize circumstances leading to GaSb melting and/or decomposition whereas creating conditions for the metathetical N for Sb element replacement *via* nitridation of the solid GaSb. From this viewpoint, other things being equal, the grain size of the powdered GaSb precursor can be one of the key factors impinging on reaction output.

3.2. Discussion of characterization data

Figure 1 shows two superimposed particle size distribution curves for the manually ground and ball milled GaSb. It is instructive to compare the two grinding ways and the sizes of the black spheres under the curves are to visualize size deterioration upon ball milling. Additionally, ball milling resulted in a quite symmetrical curve A – some 50 % of particles had diameters $d < 400$ nm and 95 % had $d < 600$ nm; practically, the particle sizes covered a narrow range of 200-700 nm. By comparison, the manually ground material showed a broad and asymmetrical curve B – some 50 % of particles had diameters $d < 12000$ nm and 95 % had $d < 30\,000$ nm; the particle sizes covered a wide range of 500-50 000 nm. It is clear that there was a significant grain size/grain surface difference between the two batches of precursor.

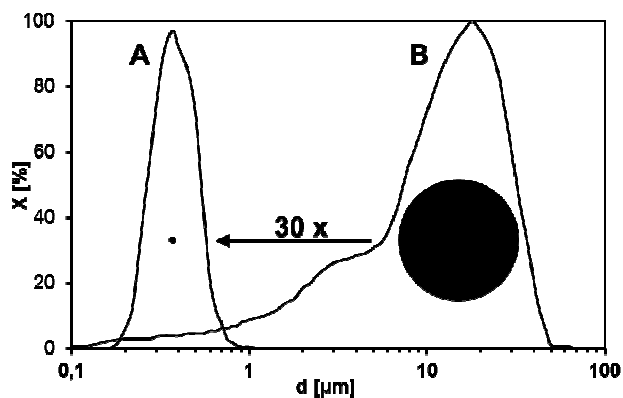


Fig. 1. Particle size distributions of ground GaSb: A – ball milled, B – manually ground. The black spheres visualize *ca.* 30-fold difference in the average particle diameters.

The representative SEM images of some of the product GaN nanopowders are shown in Figure 2. Apparently, the particle sizes on the left side (manual grinding) are on average

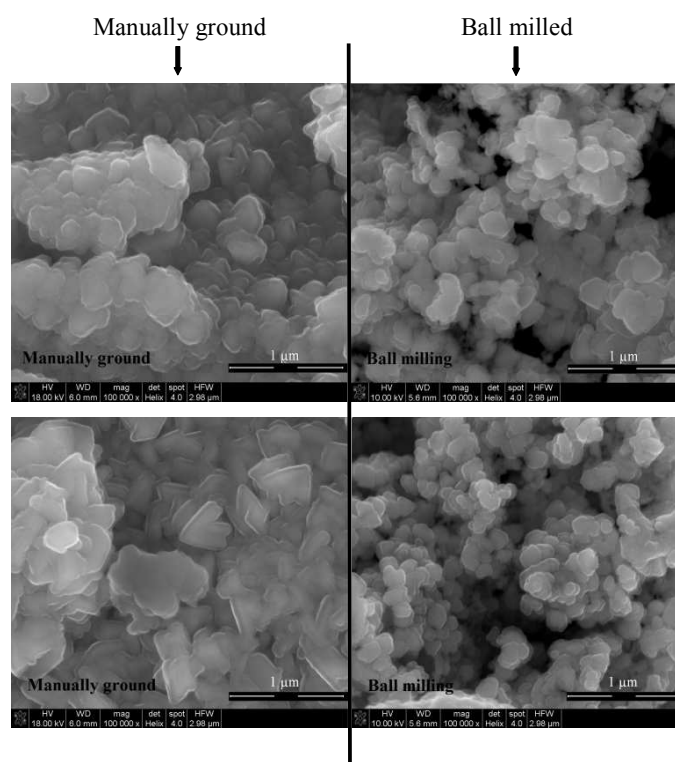


Fig. 2. SEM images of GaN nanopowders made at: top row – 900 °C, 170 h; bottom row – 1000 °C, 36 h. In both rows: left – manually ground precursor, right – ball milled precursor.

bigger than the ones on the right (ball milling). It also seems that the particles from the ball milled precursor are more size homogenous. It is to be noted that these sizes are not necessarily crystallite sizes but they rather physically represent crystallite agglomerates or mixtures of the two types of particles.⁵¹ Regarding agglomerate formation, the materials made from the manually ground GaSb consist mostly of h-GaN and those made from the ball milled GaSb include sizeable proportions of c-GaN (*vide infra*), so the smaller crystallites of c-GaN could have exerted an overall diluting effect on agglomerate formation. However, since the morphological and particle size characteristics of the ground precursor match well those of the respective nitride product (*cf.* Fig. 1 and Fig. 2), the essential role of the initial grain size features in the evolution of the nitride product morphology appears to prevail.

A set of reference and representative XRD patterns for samples prepared from the manually ground and ball milled GaSb, both from nitridation at 900 °C, 170 h, is shown in Figure 3. The relative amounts and average crystallite sizes of the GaN polytypes for all products, which were estimated from the XRD patterns are included in Table 1.

Utilization of lower reaction temperatures than 900 °C, *e.g.*, 800 and 850 °C, even with reasonably extended reaction times did not succeed in complete conversions of GaSb and both some unreacted GaSb and elemental Sb were detected in addition to GaN. Starting at 900 °C and sufficiently long times, *e.g.*, 170 h for manually ground and 90 h for ball milled GaSb, a total conversion was achieved; however, after 90 h some residual antimony was still present in the GaSb-manually ground system. In this regard, the application of high energy ball milling was beneficial by significantly cutting down the reaction time.

The proportion of the two polytypes of GaN depended strongly on temperature/time conditions as well as on the way the precursor was ground. For 900 °C and manual grinding, the longer reaction time resulted in increased quantities of the stable h-GaN with average crystallite sizes *ca.* 30 nm, *i.e.*, around 77 % after 90 h and 92 % after 170 h. This polytype

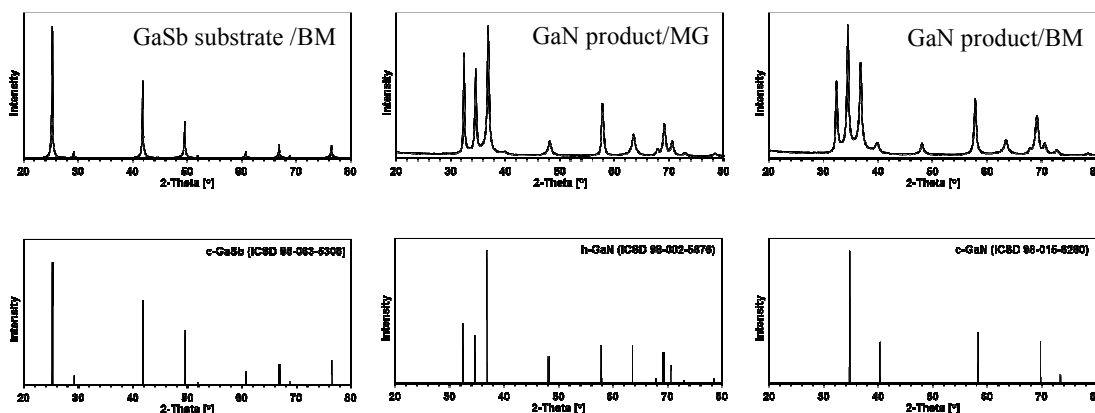


Fig. 3. XRD patterns for products from nitridation with ammonia at 900 °C, 170 h, of powdered GaSb; top left – GaSb substrate/BM, top middle – GaN product from manually ground GaSb, top right – GaN product from ball milled GaSb. MG – manually ground, BM – ball milled. Bar charts in the bottom row are for cubic GaSb (ICSD 98-063-5308) – bottom left, hexagonal h-GaN (ICSD 98-002-5676) – bottom middle, and cubic c-GaN (ICSD 98-015-6260) – bottom right.

Table 1. Amounts and average crystallite sizes of GaN polytypes (nd – not determined).

Nitridation	Grinding	h-GaN amount / av. size	c-GaN amount / av. size	Sb amount
900 °C, 90 h	manual	77.4 % / 30 nm	22.2 % / 14 nm	0.4 %
	ball milling	66 % / 23 nm	34 % / 14 nm	-
900 °C, 170 h	manual	92 % / 33 nm	8 % / nd	-
	ball milling	67 % / 25 nm	33 % / 12 nm	-
1000 °C, 36 h	manual	88 % / 33 nm	12 % / 12 nm	-
	ball milling	68 % / 24 nm	32 % / 11 nm	-

was characteristic of some preferential growth as evidenced by different values of crystallite sizes along the selected crystallographic axes ($D(010) = 41$ nm, $D(002) = 32$ nm, $D(011) = 25$ nm). Increasing the temperature to 1000 °C, 36 h, afforded 88 % of h-GaN. Interestingly, the application of ball milling resulted in the comparable quantities of h-GaN, 66-68 %,

independent on conditions. This was consistent with the high energy ball milling markedly impacting the nitridation/recrystallization phenomena in the system. The average crystallite sizes of c-GaN were in the range 11-14 nm, distinctly smaller than of h-GaN.

An additional evidence for the synthesis of GaN came from FT-IR spectra. The typical spectra for the products are shown in Figure 4, specifically, for the powders from 900 °C, 170 h. A band at 570-580 cm^{-1} is in the region typical for Ga-N stretches in GaN. A low intensity broad band at *ca.* 3450 cm^{-1} is an experimental artifact due to some water absorbed during KBr pellet preparation. Also, a curved baseline in the range 800-4000 cm^{-1} results from no specific light scattering/absorption in the opaque pellets containing gray yellowish GaN.

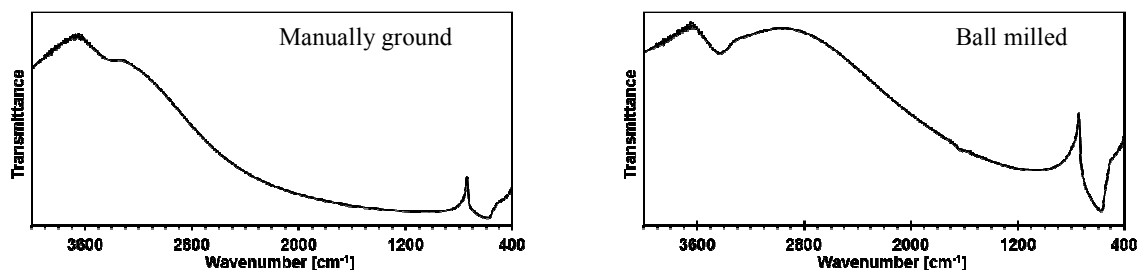


Fig. 4. FT-IR spectra for products from nitridation with ammonia at 900 °C, 170 h, of powdered GaSb; left – manually ground, right – ball milled.

The Uv-vis spectra for all product powders also supported the presence of gallium nitride. The optical spectra (absorbance vs. wavelength) for a selected set of the 1000 °C, 36 h-nitrided samples are shown in Figure 5 together with the Kubelka-Munk transformations, the latter enabling calculations of specific electronic transitions (Table 2). In this regard, the energy bandgap of the GaSb substrate is 0.726 eV that corresponds to a bandgap transition at 1707 nm, which is beyond the UV-vis range. For gallium nitride materials, E_{g1} at 3.02-3.10 eV corresponds likely to band tail transitions linked to various impurities, disorder, and

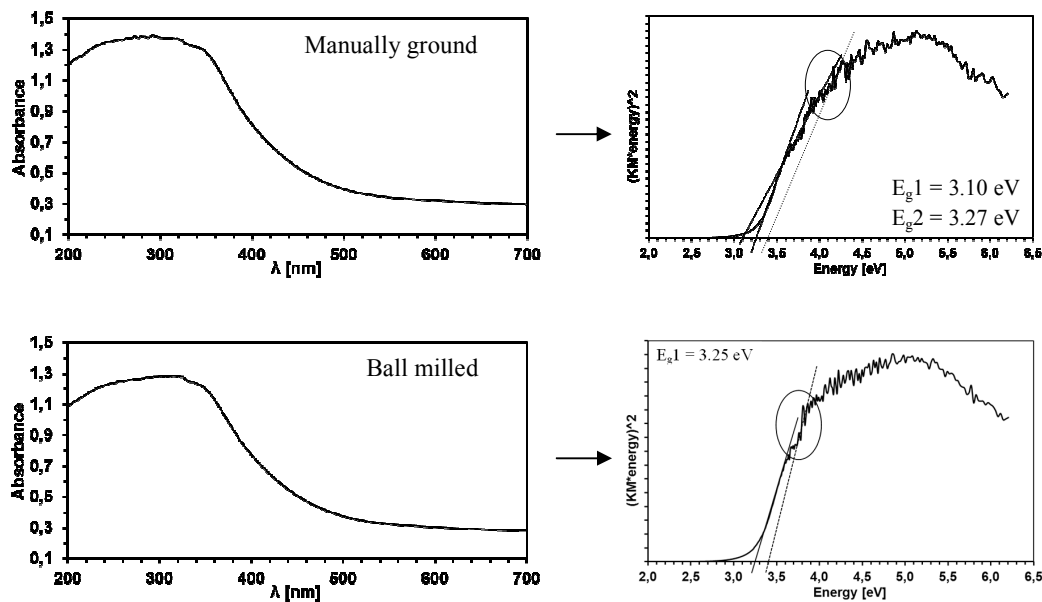


Fig. 5. Examples of UV-vis spectra of GaN from nitridation of ground GaSb, 1000 °C, 36 h; top row – manually ground, bottom row – ball milled. The left panel shows the absorbance spectra whereas the right panel includes the derived Kubelka-Munk functions.

Table 2. UV-vis derived E_g values of GaN nanopowders.

Nitridation	Grinding	E_{g1} [eV]	E_{g2} [eV]
900 °C, 90 h	manual	-	3.19
	ball milling	-	3.27
900 °C, 170 h	manual	3.03	3.25
	ball milling	3.02	3.27
1000 °C, 36 h	manual	3.10	3.27
	ball milling	-	3.25

defects and E_{g2} is related to the material's energy bandgap.¹⁶ It is interesting to note that for bulk h-GaN, the bandgap transitions are expected at around 3.4 eV whereas for c-GaN around 3.2 eV. Given the mixture of polytypes in the powders, one tentatively assigns the E_{g2} values of 3.19-3.27 eV to c-GaN. The E_{g2} values for hexagonal gallium nitride could not be unequivocally fitted in the rather noisy parts of the spectra. However, the regions shown

within the ovals in Fig. 3 could be fitted with the dotted tangent lines that consistently intersect the energy coordinate at *ca.* 3.4 eV, which is characteristic of h-GaN. This would be a rare piece of evidence from standard UV-vis determinations for the mixture of the GaN polytypes in bulk powders. It is worth to mention that GaN average crystallite sizes are larger than 3-11 nm, the values quoted for the Bohr radius of GaN¹⁷ and, therefore, no blue shift effect for E_g is expected in the current case.

A further insight into structural details of the samples was gained from the solid state ⁷¹Ga MAS NMR. The spectra for the product GaN nanopowders are shown in Figure 6 and the peak positions estimated by best-fit curve deconvolution are collected in Table 3. In no case, a resonance at -50 ppm for GaSb was detected supporting its complete conversion to GaN. From our earlier NMR studies on a range of GaN nanopowders, we concluded that a hexagonal GaN material may have two distinct gallium resonances, *i.e.*, at *ca.* 325-330 ppm and *ca.* 415-440 ppm.^{5h,18} The former peak is relatively sharp and corresponds to good crystallinity and uniformity of the short range structure order in well crystallized h-GaN. The latter peak is quite symmetrical and unusually broadened. From scarce and controversial literature data on its interpretation, the lower field broader peak has been assigned by some researchers either, in what appears a rather confusing way, to a postulated nonstoichiometric N-deficient phase GaN_{1-x} (0 < x < 1)¹⁹ or, alternatively, in what appears to us the well-substantiated reports, to a Knight shift due to the presence of conduction electrons in the semiconductor.²⁰ In our studies, we observed growing intensities of the lower field peak at the expense of the higher field peak for GaN nanopowders that were subjected to recrystallization/crystal growth by annealing at increased temperatures whereas, by comparison, no such phenomenon was detected with heating well crystalline HVPE-grown hexagonal GaN. In our opinion, the temperature-induced nanopowder recrystallization although results by XRD criteria in better crystallinity may, at the same time, introduce

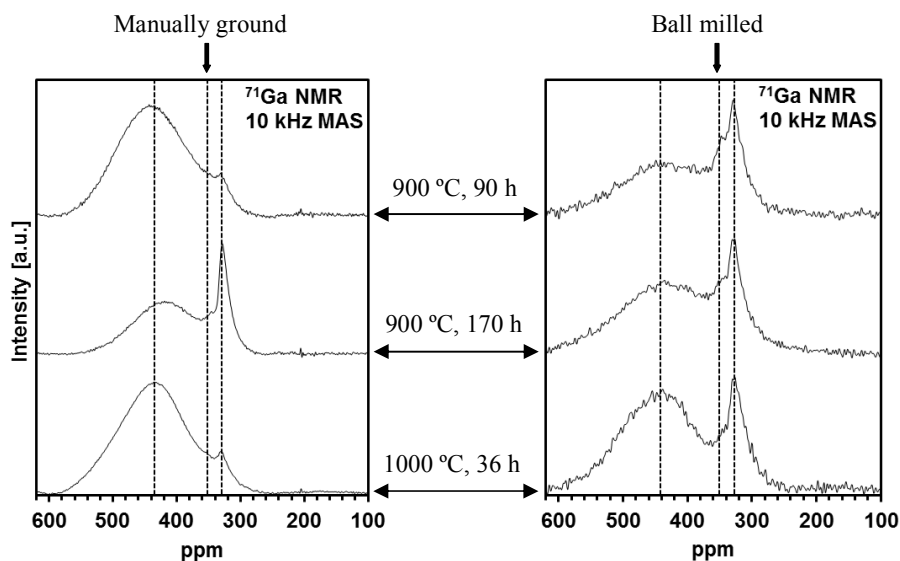


Fig. 6. Solid state ^{71}Ga MAS NMR spectra of GaN from nitridation of ground GaSb; left panel – manually ground, right panel – ball milled. Reaction temperatures and times are shown next to spectra.

Table 3. ^{71}Ga MAS NMR peak positions (n/d – not determined).

Nitridation	Grinding	High field peak [ppm]		Low field peak [ppm]	
		h-GaN	c-GaN	h-GaN	c-GaN
900 °C, 90 h	manual	330	353	445	n/d
	ball milling	331	353	439	n/d
900 °C, 170 h	manual	331	353	423	n/d
	ball milling	331	353	434	n/d
1000 °C, 36 h	manual	336	352	439	n/d
	ball milling	331	349	445	n/d

specific crystal defects including native N-defect formation and/or impurity oxygen incorporation into the crystal lattice of GaN. The interpretation of the NMR spectra is even more complex if two GaN polytypes are present. It was tentatively proposed by us that a similar set of two resonances as for h-GaN could be adequately assigned to c-GaN, *i.e.*, at

350-360 ppm^{19c,20e} and *ca.* 420-480 ppm.^{18a} In Fig. 6, clear shoulders at 350-360 ppm on the sharp peaks can be seen of which deconvolution-derived positions are included in Table 3. Such deconvolution could not, however, be reasonably applied to the symmetrical low field broad peak. This could mean that the c-GaN component in it is either absent/in small quantities (only well crystalline c-GaN is present) or the peak intensities for the two polytypes add adventitiously. In such a case, the position of the broad peak in the range *ca.* 420-480 ppm may be a rough estimate of a quantity of a selected peak's component.

For the manually ground GaSb-derived nanopowders (Fig. 6, left panel), they all show prevailing quantities of h-GaN including significant proportions of the “defected” component, the former consistent with the XRD data (see, Table 1). Among them, the 900 °C, 170 h powder is characteristic of the highest proportion of the well crystalline component of this type as judged from comparison of peak intensities in the 330 ppm range. Also, the corresponding low field peak at 423 ppm of small intensity supports a smaller quantity of the “defected” component. Interestingly, increasing the nitridation time from 90 to 170 hours results in an increased proportion of the well crystalline component of h-GaN. This is contrary to what we observed in our previous NMR study on similar GaN nanopowders where annealing at higher than the nitridation temperature caused an opposite phenomenon – the relative amount of the well crystalline component decreased.^{18a} The answer to this apparent ambiguity possibly lies in the different annealing conditions applied this time where temperature was constant and the variable was time. In such a case, the extension of annealing time results in the overall higher quantity of h-GaN with increased proportions of the well crystalline component and the latter, likely, formed from metastable c-GaN to stable h-GaN transformation whereas the h-GaN grain recrystallization stabilizes at a temperature-determined level. Such an explanation makes the XRD and NMR data consistent.

When analyzing the ball milled GaSb-derived sample data, one notices quite similar properties of their NMR spectra, now, with the relatively enhanced quantities of the c-GaN polytype. This is very much in accordance with the relevant XRD data. Compared with manual grinding, ball milling results not only in higher proportions of c-GaN but, also, in a better crystallinity of the h-GaN polytype. Increased nitridation temperatures for this pool of nanopowders are reflected in a relatively moderate increase of the “defected” component in the spectra. In essence, the application of ball milling results in GaN nanopowders that are more homogeneous and of better crystallinity supporting the essential role of GaSb grain size characteristics played in nitridation which, keeping things in proportion, conceals significantly the impact of temperature and time.

Raman spectroscopy provided yet another insight into structural properties of the nanopowders as a method being sensitive to chemical composition (purity), crystalline polytypes, and lattice defects/vacancies. The micro-Raman spectra are shown in Figure 7 and the major peaks are listed in Table 4. The spectra were subjected to best-fitting deconvolution that eventually yielded the peaks positions. In some cases of severe peak overlapping coupled with peak low intensities, *e.g.*, in the range 500-600 cm^{-1} or above 700 cm^{-1} , the deconvolution might not have substantiated the lowest intensity and broad peaks that still could be present. No spectrum contains the peaks for a potentially unconverted cubic GaSb²¹, *i.e.*, 228 cm^{-1} (TO mode) and 238 cm^{-1} (LO mode), which is consistent with efficient nitridation.

A striking feature of all the spectra is that the highest intensity peak is at *ca.* 150 cm^{-1} that is assigned to the $E_2(\text{low})$ phonon mode in GaN,^{22a-d} which is rather uncommon among various gallium nitride materials. This peak is in some cases asymmetrical and results in two deconvoluted components. In this regard, the sharpness and high intensity of the $E_2(\text{low})$ peak in related wurzitic ZnO films were attributed to increased crystal quality,²³ in our case well

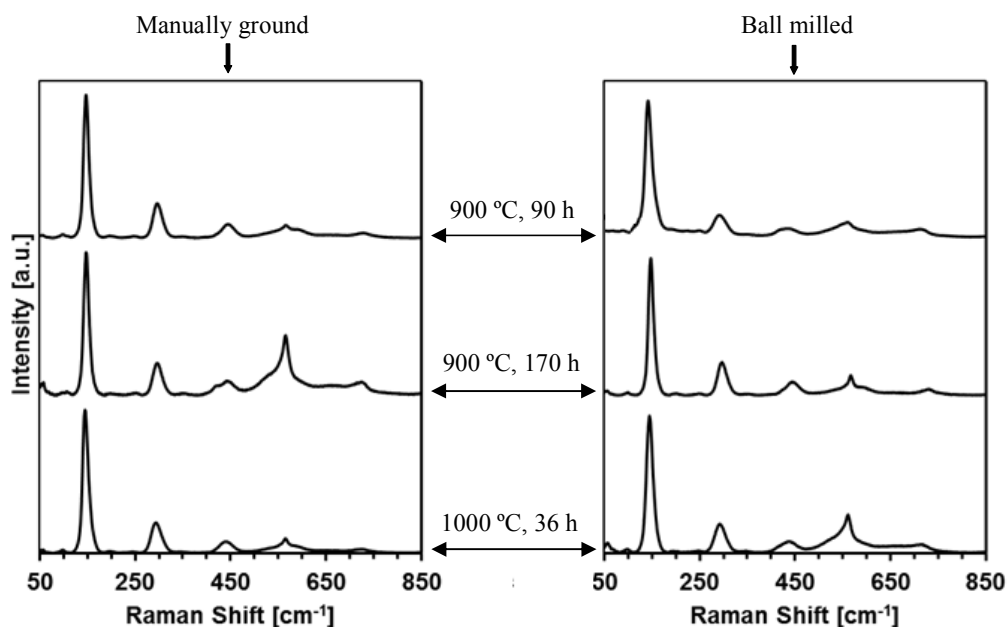


Fig. 7. Raman spectra of GaN from nitridation of ground GaSb; left panel – manually ground, right panel – ball milled. Reaction temperatures and times are shown next to spectra.

agreeing with the relevant XRD data. The $E_2(\text{low})$ phonon mode is specific for hexagonal GaN and the presence of two peaks in this range can be related to two peaks for the h-GaN component in the gallium NMR spectra. One of the two well crystalline h-GaN varieties may be stoichiometric (sharper higher field NMR peak) whereas the other one may be N-deficient/N-defected (broader lower field NMR peak), speaking in terms of explanations offered by NMR determinations (*vide supra*). Also, an unexpected feature in all spectra is the presence of two medium intensity peaks at *ca.* 300 cm^{-1} and *ca.* 440 cm^{-1} some of which are deconvoluted into two components. Literature interpretation of the 300 cm^{-1} peak has involved either a lower symmetry activation of the otherwise silent $B_1(\text{low})$ mode in h-GaN^{22e,f} or its assignment to the host lattice vibrational states^{22g} whereas the peak around 440 cm^{-1} has been proposed to result from nitrogen vacancy-related defects.^{22g} It is appropriate to mention here that another peak at $659\text{--}671\text{ cm}^{-1}$ was also attributed to nitrogen defects^{22a,d,g} although $B_1(\text{high})$ activated mode was proposed as well.^{22f} Generally, the presence of the N-

Table 4. Positions of deconvoluted peaks in micro-Raman scattering determinations for GaN nanopowders. Two symmetry allowed modes for c-GaN are shown in italics.

Mode assignment range	Raman shift [cm^{-1}]					
	From manually ground precursor			From ball milled precursor		
	900 °C 90 h	900 °C 170 h	1000 °C 36 h	900 °C 90 h	900 °C 170 h	1000 °C 36 h
$E_2(\text{low})$ [22a-d]	147	148	145 153	141 151	147 150	144 156
$B_1(\text{low})$ silent [22e, f], host lattice vibrations [22g]	297	297	292 309	293	296 311	292 308
Nitrogen vacancies [22g]	445	418 444	440	433	421 445	435
$A_1(\text{TO})$, $E_1(\text{LO})$, $E_2(\text{high})$ [22a-d], <i>TO(c-GaN)</i> [22b, d]	541 - 565 589	539 552 566 594	545 554 565 585	545 - 560 590	549 555 567 593	526 549 561 574
$B_1(\text{high})$ silent [22f], nitrogen vacancies [22a, d, g]	668	671	661	668	659	667
$A_1(\text{LO})$, $E_1(\text{TO})$ [22a], <i>LO(c-GaN)</i> [22b, d]	727	723	725	714	729	715

defect related peaks conforms well with the ^{71}Ga MAS NMR data and the N-deficient phase peaks there.

The Raman spectra contained also all other allowed peaks for both GaN polytypes, *i.e.*, for h-GaN – $A_1(\text{TO})$, $A_1(\text{LO})$, $E_1(\text{LO})$, $E_1(\text{TO})$, $E_2(\text{high})$ and for c-GaN – TO and LO modes. Somehow, unfortunately, many of them lie very close to others and may, therefore, merge and, at the same time, their assignment may be rather ambiguous. This is the situation of the region *ca.* 530-600 cm^{-1} where four peaks are expected and above 700 cm^{-1} where three peaks can occur for two polytypes as shown in Table 4. That is why in the region *ca.* 530-600 cm^{-1}

the positions of the deconvoluted peaks are included without a strict assignment of each phonon mode while, generally, they confirm the presence of two GaN polytypes. In the region above 700 cm^{-1} , there is only one deconvoluted peak but given the peak's small intensity and broadness other components may be just unresolved. In this regard, the $A_1(\text{LO})$ mode there has been reported to be absent in GaN samples with high free-carrier concentrations.^{22g} In summary of this aspect, the Raman spectra for all samples were of very good quality and all major modes for two GaN polytypes were resolved with low background noise in the entire spectral range. This was consistent with high purity and very good crystallinity of GaN.

From the discussion of all the characterization data, it is evident that only the combination of various methods, for instance, such as XRD diffractometry and UV-vis, Raman, and NMR spectroscopies can provide a comprehensive description of the GaN nanopowder structures with unquestionably diverse intrinsic properties. In this regard, the application of high resolution TEM may in favorable cases be extremely useful, especially, to visualize cases of intra-growth of regular and hexagonal domains within a nanograin but such an approach was outside the scope of this project.

3.3. Pathways in ammonolysis of GaSb

The overall picture that emerges from this study involves a specific reactivity pattern in ammonolysis of GaSb which includes two concurrent in many respects pathways – one which leads to metastable cubic GaN likely *via* formation of transient cubic GaSb_xN_y species and another which results in stable hexagonal GaN *via* ammonolysis of molten/decomposed GaSb. An outstanding problem beyond the scope of this work is a temperature dependent dynamics of c-GaN to h-GaN transformation in bulk powders which has not yet been fully addressed in the literature. Figure 8 graphically depicts the proposed sequence of major events that is supported by the experimental data.

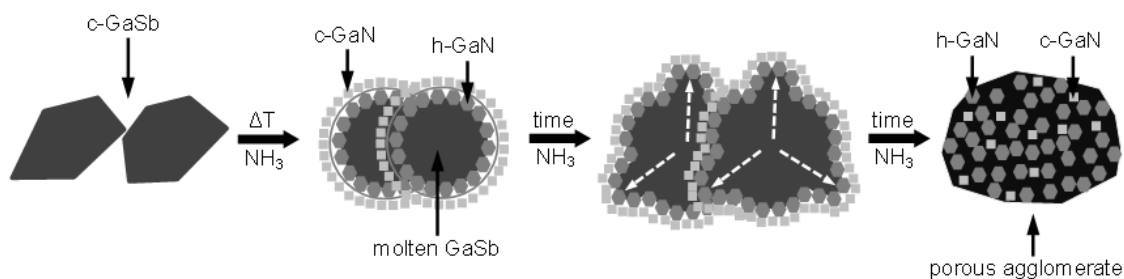


Fig. 8. Ammonolytical nitridation of microcrystalline particles of c-GaSb to mixtures of nanocrystalline particles of h-GaN and c-GaN.

In the initial nitridation stages, solid layers of short lived/unstable $c\text{-GaSb}_x\text{N}_y$ are proposed to form first on c-GaSb particle surfaces, which efficiently undergo further ammonolysis towards metastable c-GaN. This stage is topochemically controlled and decides about the final relative amounts of the cubic polytype. Simultaneously, upon reaching the melting point of GaSb at 712 °C, the particle core melts and diffusion controlled ammonolysis of molten GaSb produces the stable h-GaN in admixture with Sb. The in and out gas/vapor fluxes cause, eventually, particle deterioration and mixing of the two GaN polytypes into agglomerates. Increasing the reaction time at 900 °C from 90 to 170 hours results in increased proportions of the stable h-GaN, possibly, *via* thermodynamically supported and relatively slow c-GaN to h-GaN transformation. Eventually, for the manually ground GaSb the mixtures of both GaN polytypes with predominant h-GaN are produced and the latter amounts to 77-92 % depending on nitridation temperature and time. Deeper grinding of GaSb by high energy ball milling shortens the effective reaction time and provides nanopowders with surprisingly stable c-GaN to h-GaN proportions in all products, *i.e.*, with h-GaN in the range 66-68 % suppressing greatly the time/temperature effect. It appears that the overall long nitridation times in the studied temperature range, especially at 900 °C, are determined to a great extent by a rather slow removal of antimony by-product vapors from the system.

4. Conclusions

The ammonolytical nitridation of GaSb constitutes a new convenient way for a one-stage preparation of h-GaN-rich nanopowders of high purity, very good crystallinity, and controlled c-GaN to h-GaN proportions under the relatively conservative conditions. The concurrent formation of the metastable cubic GaN is consistent with topochemistry playing a significant role in the nitridation of cubic GaSb, in which it competes with the thermodynamically supported pathways leading to the stable hexagonal GaN. The latter is supported by ammonolysis of the molten GaSb and/or liquid Ga from thermally induced decomposition of GaSb, both events virtually unavoidable at practical reaction temperatures, whereas the former appears to be a function of a rate of ammonolysis of the solid GaSb. From this point of view, controlling these factors is a key to an engineered synthesis of the GaN polytypes. In this regard, one of the essential factors is the GaSb substrate particle size/particle surface area which is determined by a grinding method.

A more comprehensive description of the formation and stability of both GaN polytypes in the *in statu nascendi* prepared nanopowders requires additional studies on c-GaN vs. h-GaN equilibria in function of crucial experimental parameters such as temperature, time, and kind of gas atmosphere. An intriguing question of a frequently interrelated intra-growth of the cubic and hexagonal domains in a nitride nanograin has also to be addressed. Such studies are planned in our laboratory in the near future.

Acknowledgement. The study was supported by the Polish National Science Center (NCN), Grant No. 2013/09/B/ST5/01223.

References

1. a) I. Akasaki, *Angew. Chem. Int. Edit.*, 2015, **54(27)**, 7750-7763; b) H. Amano, *Angew. Chem. Int. Edit.*, 2015, **54(27)**, 7764-7769; c) S. Nakamura, *Angew. Chem. Int. Edit.*, 2015, **54(27)**, 7770-7788; d) S. S. Khludkov, I. A. Prudaev, O. P. Tolbanov, *Rus. Phys. J.*, 2013, **55(8)**, 903-909; e) M. S. Kang, C. H. Lee, J. B. Park, H. Yoo, G. C. Yi, *Nano Energy*, 2012, **1(3)**, 391-400.
2. a) T. Hashimoto, E. Letts, S. Hoff, *Sensor. Mater.*, 2013, **25(3)**, 155-164; b) R. Dwilinski, R. Doradzinski, J. Garczynski, L. Sierzputowski, R. Kucharski, M. Zajac, M. Rudzinski, R. Kudrawiec, W. Strupinski, J. Misiewicz, *Phys. Status Solidi A*, 2011, **208(7)**, 1489-1493; c) M. Bockowski, P. Strak, I. Grzegory, S. Porowski, *Technology of gallium nitride crystal growth*, Book Series: Springer Series in Materials Science, 2010, vol. 133, pp. 207-234; d) V. Avrutin, D. Silversmith, Y. Mori, F. Kawamura, Y. Kitaoka, H. Morkoc, *Proc. IEEE*, 2010, **98(7)**, 1302-1315.
3. a) M. A. Malik, M. Afzaal, P. O'Brien, *Chem. Rev.*, 2010, **110**, 4417-4446; b) B. Mazumder, A. L. Hector, *J. Mater. Chem.*, 2009, **19**, 4673-4686; c) C. N. R. Rao, C. R. C. Vivekchand, K. Biswas, A. Govindaraj, *Dalton T.*, 2007, 3728-3749; d) J. A. Jegier, S. McKernan, A. P. Purdy, W. L. Gladfelter, *Chem. Mater.*, 2000, **12**, 1003-1010; e) R. L. Wells, W. L. Gladfelter, *J. Clust. Sci.*, 1997, **8(2)**, 217-238.
4. R. L. Wells, J. F. Janik, *Eur. J. Solid State Inorg. Chem.*, 1996, **33**, 1079-1090.
5. a) J. F. Janik, R. L. Wells, *Chem. Mater.*, 1996, **8**, 2708-2711; b) J. L. Coffey, M. A. Johnson, L. Zhang, R. L. Wells, J. F. Janik, *Chem. Mater.*, 1997, **9**, 2671-2673; c) J. F. Janik, R. L. Wells, J. L. Coffey, J. V. St. John, W. T. Pennington, G. L. Shimek, *Chem. Mater.*, 1998, **10**, 1613-1622; d) J. L. Coffey, T. W. Zerda, R. Appel, R. L. Wells, J. F. Janik, *Chem. Mater.*, 1999, **11**, 20-22; e) L. Czepirski, J. F. Janik, E. Komorowska-Czepirska, R. L. Wells, *Adsorpt. Sci. Technol.*, 2002, **20**, 723-728; f) R. L. Jouet, A. P. Purdy, R. L. Wells, J. F. Janik,

- J. Clust. Sci.*, 2002, **13**, 469-486; g) J. F. Janik, *Powder Technol.*, 2005, **152**, 118-126; h) M. Drygas, Z. Olejniczak, E. Grzanka, M. M. Bucko, R. T. Paine, J. F. Janik, *Chem. Mater.*, 2008, **20**, 6816-6828; i) M. Drygas, J. F. Janik, *Mater. Chem. Phys.*, 2012, **133**, 932-940.
6. J. F. Janik, R. L. Wells, *Inorg. Chem.*, 1997, **36**, 4135-4137.
7. a) G. L. Wood, E. A. Pruss, R. T. Paine, *Chem. Mater.* 2001, **13**, 12-14; b) J. F. Janik, M. Drygas, S. Stelmakh, E. Grzanka, B. Palosz, R. T. Paine, *Phys. Stat. Sol. A*, 2006, **203**, 1301-1306.
8. a) S. Stelmakh, A. Swiderska-Sroda, G. Kalisz, S. Gierlotka, E. Grzanka, B. Palosz, M. Drygas, J. F. Janik, R. T. Paine, *Proceedings of the International Conference on Nanoscience and Technology*, Basel, Switzerland, July 30-Aug 4, 2006 - Institute of Physics Publishing: Philadelphia, PA, 2006; b) E. Grzanka, S. Stelmakh, S. Gierlotka, A. Swiderska-Sroda, G. Kalisz, B. Palosz, M. Drygas, J. F. Janik, R. T. Paine, *European Powder Diffraction Conference, EPDIC-10*, Geneva, Switzerland, Sept. 1-4, 2006 - *Z. Kristallogr.* 2007, **26**, MS11-P2; c) J. Borysiuk, P. Caban, W. Strupinski, S. Gierlotka, S. Stelmakh, J. F. Janik, *Cryst. Res. Technol.*, 2007, **42**, 1291-1296; d) Polish patent No. P-378458: Way to make sintered gallium nitride GaN; patent issued as published in *Wiadomości Urzędu Patentowego* (News of the Polish Patent Office), No. 2/2012, Feb. 29, 2012.
9. a) A. Addamiano, *J. Electrochem. Soc.*, 1961, **108(11)**, 1072-1072; b) W. S. Jung, O. H. Han, S. A. Chae, *Mater. Chem. Phys.*, 2006, **100**, 199-202; c) M. Drygas, M. M. Bucko, E. Grzanka, J. F. Janik, *Curr. Nanosci.*, 2013, **9**, 173-182.
10. J. W. Hwang, J. P. Campbell, J. Kozubowski, S. A. Hanson, J. F. Evans, W. L. Gladfelter, *Chem. Mater.*, 1995, **7(3)**, 517-525.
11. M. A. Todd, G. Bandari, T. H. Baum, *Chem. Mater.*, 1991, **11(3)**, 547-551.
12. J. Deslippe, S. G. Louie, in *Comprehensive Semiconductor Science and Technology*, eds. P. Bhattacharya, R. Fornari, H. Kamimura, Elsevier, 2011, chapter: *Ab initio theories of the*

structural, electronic, and optical properties of semiconductors: bulk crystals to nanostructures, p. 51.

13. a) A. Mondal, T. D. Das, N. Halder, S. Dhar, J. Kumar, *J. Cryst. Growth*, 2001, **297**, 4-6; b) V. L. Berkovits, A. B. Gordeeva, T. V. L'vova, V. P. Ulin, *Semiconductors*, 2012, **46(11)**, 1432-1436; c) D. Wang, S. P. Svensson, L. Shterengas, G. Belenky, C. S. Kim, I. Vurgaftman, J. R. Meyer, *J. Appl. Phys.*, 2009, **105**, 014904; d) L. Buckle, B. R. Bennett, S. Jollands, T. D. Veal, N. R. Wilson, B. N. Murdin, C. F. McConville, T. Ashley, *J. Cryst. Growth*, 2005, **278**, 188-192; e) J. Buckeridge, D. O. Scanlon, T. D. Veal, M. J. Ashwin, A. Walsh, C. R. Catlow, *Phys. Rev. B*, 2014, **89**, 014107.
14. a) C. Y. Yeh, Z. W. Lu, S. Froyen, A. Zunger, *Phys. Rev. B*, 1992, **46(16)**, 10086-10097; b) A. Zoroddu, F. Bernardini, P. Ruggerone, V. Fiorentini, *Phys. Rev. B*, 2001, **64**, 045208.
15. S. Suandon, S. Sanorpim, K. Yoodee, K. Onabe, *Thin Sol. Films*, 2007, **515(10)**, 4393-4396.
16. I. Akyuz, S. Kose, F. Atay, V. Bilgin, *Semicond. Sci. Technol.*, 2006, **21**, 1620-1626.
17. a) P. Ramvall, S. Tanaka, S. Nomura, P. Riblet, Y. Aoyagi, *Appl. Phys. Lett.*, 1998, **73(8)**, 1104-1106; b) X. L. Chen, J. N. Li, Y. G. Cao, Y. C. Lan, H. Li, M. He, C. Y. Wang, Z. Zhang, Z. Y. Qiao, *Adv. Mater.*, 2000, **12(19)**, 1432-1434.
18. M. Drygas, M. M. Bucko, Z. Olejniczak, I. Grzegory, J. F. Janik, *Mater. Chem. Phys.*, 2010, **122**, 537-543.
19. a) W. S. Jung, C. Park, S. Han, *Bull. Korean Chem. Soc.*, 2003, **24(7)**, 1011-1013; b) W. S. Jung, *Mater. Lett.*, 2006, **60**, 2954-2957; c) W. S. Jung, O. H. Han, S. A. Chae, *Mater. Chem. Phys.*, 2006, **100**, 199-202; d) B. Schwenzer, J. Hu, R. Seshadri, S. Keller, S. P. DenBaars, U. K. Mishra, *Chem. Mater.*, 2004, **16**, 5088-5095; e) B. Schwenzer, J. Hu, Y. Wu, U. K. Mishra, *Solid State Sci.*, 2006, **8**, 1193-1201.

20. a) J. P. Yesinowski, A. P. Purdy, *J. Am. Chem. Soc.*, 2004, **126**, 9166-9167; b) J. P. Yesinowski, A. P. Purdy, *J. Am. Chem. Soc.*, 2006, **128**, 4952-4953; c) J. P. Yesinowski, *Phys. Status Solidi C*, 2005, **2(7)**, 2399-2402; d) J. P. Yesinowski, A. P. Purdy, H. Wu, M. G. Spencer, J. Hunting, F. J. DiSalvo, *J. Am. Chem. Soc.*, 2006, **128**, 4952-4953; e) J. P. Yesinowski, in *Solid State NMR Book Series: Topics in Current Chemistry*, Springer, 2012, vol. 306, ed. J. C. C. Chan, chapter: *Solid-state NMR of inorganic semiconductors*, pp. 229–312.
21. S. V. Demishev, Y. V. Kosichkin, A. G. Lyapin, N. N. Mel'nik, D. V. Nekhaev, N. E. Sluchanko, O. A. Turok, *JETP*, 1993, **77(2)**, 329-336.
22. a) M. Gopalakrishnan, V. Purushothaman, P. S. Venkatesh, V. Ramakrishnan, K. Jeganathan, *Mater. Res. Bull.*, 2012, **47**, 3323-3329; b) Y. S. Wu, W. K. Chang, H. Y. Lai, *J. Cryst. Growth*, 2008, **310**, 2800-2805; c) M. S. Kumar, J. Kumar, *Mater. Chem. Phys.*, 2002, **77**, 341-345; d) H. Harima, *J. Phys.: Condens. Matter.*, 2002, **14**, R967-R993; e) A. Hushur, M. H. Manghnani, J. Narayan, *J. Appl. Phys.*, 2009, **106**, 054317; f) F. J. Manjóna, B. Marí, J. Serrano, A. H. Romero, *J. Appl. Phys.*, 2005, **97**, 053516; g) M. Katsikini, K. Papagelis, E. C. Paloura, S. Ves, *J. Appl. Phys.*, 2003, **94**, 4389-4394.
23. C. Wang, Z. Chen, Y. He, L. Li, D. Zhang, *Mater. Sci.-Poland*, 2010, **28(1)**, 153-161.